Colloid Polym Sci 279: 376–381 (2001)

SHORT COMMUNICATION

P. Müller-Buschbaum
M. Stamm

Film thickness dependence of the domain size in weakly incompatible thin polymer blend films

Received: 27 July 2000
Accepted: 30 October 2000

P. Müller-Buschbaum (✉)
TU München, Physik-Department
LS E13, James-Franck-Str.1
85747 Garching
Germany
e-mail: muellerb@physik.tu-muenchen.de
Tel.: 089-289-12450; Fax: 089-289-12473

M. Stamm
Institut für Polymerforschung e.V. (IPF)
Hohe Str. 6, 01069 Dresden
Germany

Abstract The surface morphology of thin polymer blend films of deuterated polystyrene (dPS) and polyparamethylstyrene (PpMS) is investigated with scanning force microscopy (SFM) and optical microscopy. From a statistical analysis of the data the most prominent in-plane length picturing the domain size as a function of the blend film thickness is determined. In ultra-thin films surface patterns directly after preparation are absent, whereas for thicker films a linear dependence is observed. After a relaxation towards equilibrium, resulting from annealing or storage under toluene vapor, the power law observed changes for ultra-thin films and remains unchanged for thicker films.

Key words Scanning force microscopy · Thin films · Polymer blends

Polymer blends are extensively used in many applications to obtain specially designed properties that are not accessible with homopolymers. With the need of ongoing miniaturization, polymer-blend films are being prepared with decreasing film thickness. While for larger film thicknesses surface directed spinodal decomposition creates an internal ordering of the blend film [1], below a critical thickness this mechanism is suppressed [2]. The long-range force of the substrate [3] becomes important and surface morphologies are created [4–11]. The actual type of surface morphology is determined by the competition between diffusive and hydrodynamic growth [12]. Therefore, the polymer-polymer interaction parameter [13], the blend composition [14], and the polymer viscosity [12] are important parameters. A large number of investigations focuses on the installed morphologies [4–11] and on the kinetics of domain growth [15–18]. Recently, a cross-over from a 3D to a 2D behavior was identified from a change in the growth exponent [18]. In the present investigation we determine the evolving characteristic in-plane length scale of the surface morphology as a function of blend film thickness. To include on one hand the effects of confined geometry and to exclude on the other hand the surface directed spinodal decomposition, we prepared film thicknesses between $R_g/3$ and 26 R_g, where R_g denotes the radius of gyration of the unperturbed polymer molecule (about 100 Å for the used polymers). Towards smaller film thickness $R_g/3$ marks the lower limit that can be prepared as a homogeneous film. Films with $R_g/4$, for example, remain incomplete after preparation.

Different film thicknesses are prepared by a variation of the polymer concentration of the toluene solution used during the spin-coating process [19]. The preparation of thin films with the spin-coating technique enables the control of the resulting film thickness with high accuracy. We used deuterated polystyrene (dPS) with a molecular weight $M_w = 157$ kg/mol ($M_w/M_N = 1.09$, $R_g = 106$ Å) as well as polyparamethylstyrene (PpMS) with a molecular weight $M_w = 157$ kg/mol ($M_w/M_N = 1.06$, $R_g = 100$ Å) in an asymmetric blend composition of PpMS:dPS = 60:40. The surface tension of dPS $\gamma(dPS) = 40.7$ mN/m^2 [20] is larger than that of PpMS $\gamma(P\text{pMS}) = 35.0$ mN/m^2 [21]. As determined recently [22], the resulting surface morphologies are continuous patterns, which are easily distinguishable from typical dewetting patterns like holes, continuous rim structures or drops [23, 24]. Both polymers differ only by one methyl group. Thus, the blend system is only weakly incompatible. For the bulk system

PpMS:dPS a polymer-polymer interaction parameter $\chi = A + B/T$ with A = −0.011 ± 0.002 and B = 6.8 ± 1 K [25] (yields $N\chi \cong 6.6$) was determined. Prior to spin-coating (1950 rpm for 30 s) the silicon Si(100) substrates were cleaned in a bath of 100 ml of 80% H_2SO_4, 35 ml H_2O_2 and 15 ml deionized water for 15 minutes at 80 °C, rinsed in deionized water and dried with compressed nitrogen. Right after preparation the samples were examined with X-ray reflectivity to determine the prepared film thickness and to prove the presence of a homogeneous polymer blend film on top of the substrate. In addition, samples were annealed 8 h and 62 h at $T = 161$ °C in a vacuum furnace or stored for 7 h under a toluene atmosphere. Next, they were quenched down to room temperature and ambient air. The annealing temperature is above the glass transition temperature of both polymers and within the unstable regime of the dPS/PpMS phase diagram. Both annealing times are inside the time range during which phase separation is dominant as compared to dewetting [8]. From the X-ray reflectivity measurements we can exclude a surface-directed spinodal decomposition. The storage under a toluene atmosphere after the preparation lowers the glass transition temperature [26]. The polymer layer is swollen by the incorporated toluene molecules from the surrounding atmosphere, which act as a plasticizer. The film thickness is increased by 20%. The original homogeneous polymer film is replaced by a highly concentrated PpMS:dPS-toluene solution layer. Therefore, the viscosity and surface tension are reduced. In addition, the long-range interaction changes. The polymer-substrate van der Waals interaction is replaced by the polymer/toluene-substrate interaction. This changes the effective Hamaker constant of the system [27].

In general, the spin coating process is described within a three-step model [28]. During the first step most of the solution is spun-off. A radial outflow of highly concentrated solution dominates the second step, ending with a film thickness h_w. In the third step only solvent evaporation reduces the film thickness down to the dry film thickness $l = (1 - x_0)h_w$ which is measured in our experiment [29]. The initial solvent mass fraction

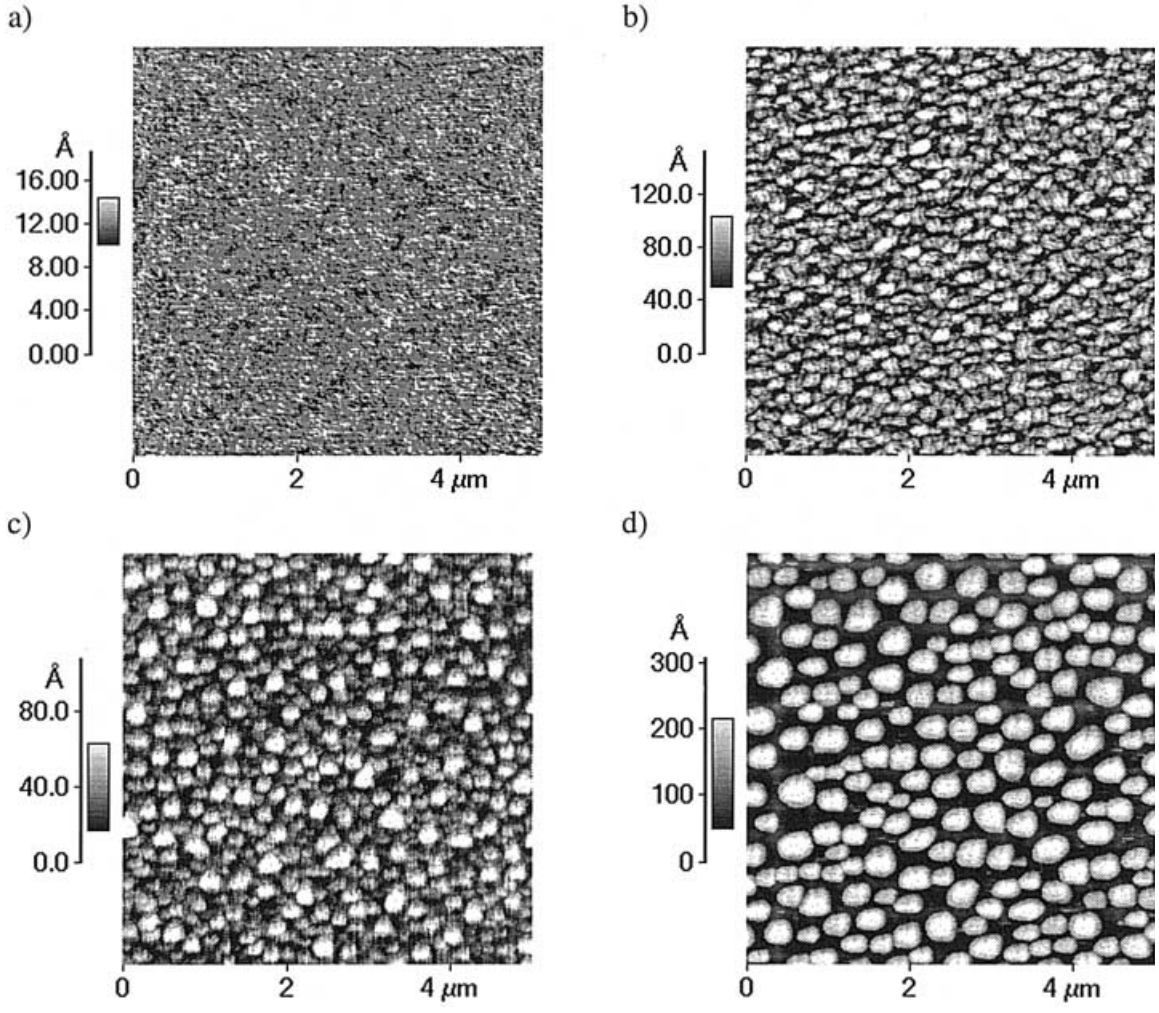

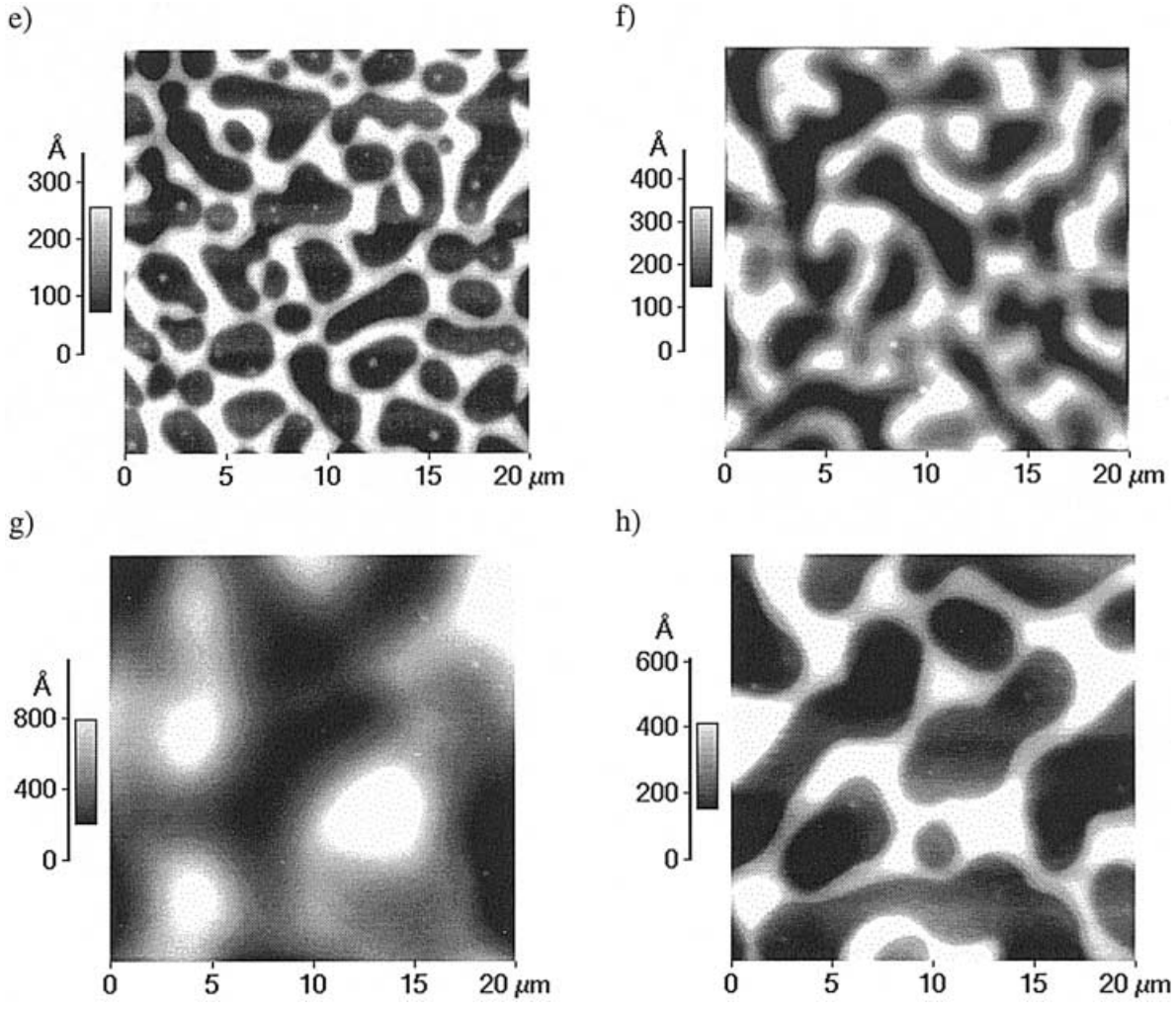

Fig. 1 SFM pictures of the topology of blend films as prepared (*a*, *e*), after 8 h annealing (*b*, *f*), 62 h annealing (*c*, *g*) and toluene vapor storage (*d*, *h*). For the confined thin films with a film thickness of $R_g/3$ (*a–d*) a small scan range of 5 μm × 5 μm and for the thick films with a film thickness of 26 R_g (*e–h*) a scan range of 20 μm × 20 μm is shown to clarify the measured morphologies. In each SFM graph the gray scale is individually chosen to emphasize the surface pattern

in the coating solution is denoted with x_0. The observed morphologies are created during the diffusion-controlled third step. Due to the deep quench, a once created phase separation morphology is frozen in [30]. Within the extremely small time window of the spin coating process no morphological changes are possible. Thus, right after preparation the samples are in a non-equilibrium but well-defined state. The investigated intermediate states after annealing or toluene storage can be understood as snap-shots of the ongoing process. It is driven by the minimization of the excess surface free energy density of the system. In contrast to the well investigated time dependence [15, 18], we focus in the present investigation on the film thickness dependence.

Four different samples of each film thickness were investigated to ensure reproducibility of the results. After each preparation, within the experimental error, we observe equal film thicknesses and surface morphologies. The surface morphology of the as prepared as well as of the quenched samples was examined with a scanning force microscope (PARK Autoprobe CP). Operating in non-contact mode several images between 0.5 μm × 0.5 μm and 100 μm × 100 μm were obtained. The data were recorded at room temperature under air. We used gold-coated silicon cantilevers with a sharp, asymptotic conical tip with a high aspect ratio (PARK Ultralevers) which are well suited for the investigation of tall structures. To detect possible larger structures and resolve the evolving large morphologies with sufficient statistics, in addition optical microscopy (Zeiss Axiotech 25H) with magnifications between 4 times and 50 times was performed.

Fig. 1 shows as an example of the observed morphologies of ultra-thin films (Fig. 1a–d: thickness $l = R_g/3$) and of thick films (Fig. 1e–h: thickness $l = 26\ R_g$)

right after preparation, after 8 h and 62 h annealing and after toluene vapor storage. Obviously there are remarkable differences: Samples with $l < R_g$ exhibit a flat and featureless surface after preparation. After annealing or toluene treatment small droplets are present at the surface. The droplet diameter as well as the droplet distances depend on the sample treatment (annealing/vapor storage). In contrast, films with $l > R_g$ show a continuous surface pattern right after preparation. After annealing the structure has coarsened but is still continuous. The observed surface patterns are very similar to the calculated ones with a conserved order parameter [12]. In reference [12] based on a lattice Boltzmann simulation the coarsening of the domains in phase-separating binary fluids is investigated. In case of high viscosity and negligible hydrodynamic flow the experimentally observed morphologies fit well to the calculated ones. This strongly suggests that in the case of the blend system PpMS:dPS examined in this investigation, the coarsening is not dominated by hydrodynamic flow. In contrast for PMMA:PS blend films hydrodynamic flow was attributed to be the leading mechanism during the coarsening of the as cast blend film [9]. The differences in the investigated molecular weights which change the viscosity as well as the change in the polymer-polymer interaction parameter might be a reason for this observation. For samples with $l > 2R_g$ even after the plastification the continuous structure remains. Thus, during the plastification the viscosity was still so high that hydrodynamic flow can be neglected.

To obtain a statistical description, the SFM and the optical micrograph data of individual scan ranges were Fourier transformed, yielding a 2D intensity information in reciprocal space quite similar to a scattering signal. Because in optical micrographs in addition to the xy-coordinate the third information is a color value only and not a height information like in SFM data, both Fourier transformed data sets differ in the meaning of the intensity axis. From the appearance of a Fourier ring the rotational isotropy of the surface morphologies and the existence of one most prominent in-plane length can be concluded. After radial averaging, power spectral density functions (PSDs) with a limited q-range result. The combination of the PSD with different q-ranges, corresponding to individual scan ranges, yields a master curve. We restrict this combination to PSD resulting from one experimental method, either SFM or optical microscopy. Each master curve statistically describes the measured surface morphology with an increased q-range as compared to an individual PSD [22]. The actual value of the most prominent in-plane length Λ is determined from the position of the maximum $q_{max} = 2\pi/\Lambda$ of the master curve [13]. This works irrespective of the originally applied technique, SFM or optical microscopy.

Fig. 2 shows Λ as a function of blend film thickness l right after preparation. It has to be noted that l resembles the dry film, although the phase separation process occurs at a different, larger film thickness. The absence of a surface pattern yields a master curve without any peak which we identify with $\Lambda = 0$ [22]. On basis of a mean-field treatment it was theoretically predicted that with decreasing film thickness the polymer-polymer interaction parameter is decreased as well [31] and thus polymer-blend films become more compatible [32]. As recently shown, the characteristic in-plane length of a surface blend morphology decreases with increasing compatibility for as prepared films [13]. Therefore, we can attribute the increase of Λ with increasing film thickness to the decreasing compatibility. For equilibrium thin-blend films, the existence of a critical film thickness below which surface pattern evolution is suppressed [33], is theoretically predicted. Of course, as prepared thin blend films are far away from equilibrium as the evolution of surface morphologies after annealing demonstrate. Furthermore, for polymer blend films a drastic change in many physical properties, resulting from the spatial restriction, like deviations in the glass transition temperature and chain mobility as compared to bulk values or an diffusion anisotropy [34–37], were reported. Thus, it might be reasonable that this non-monotonous behavior is originated by a spatial restriction of the film thickness, which suppresses a lateral phase separation [19] for $l < R_g$.

Using a double logarithmic plot in Fig. 3 the data of the as prepared as well as of the treated samples are shown. The samples yielding $\Lambda = 0$ are skipped. The

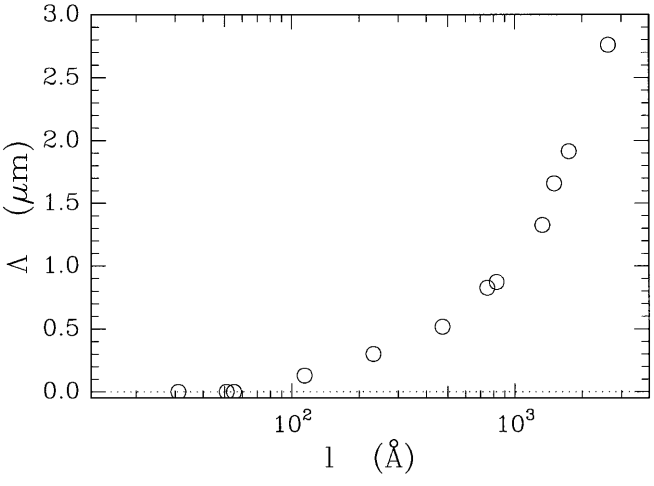

Fig. 2 Characteristic in-plane length Λ as a function of the dry polymer blend film thickness l for the as prepared samples. Note that the morphologies are created at a film thickness which is larger than l. Master curves of SFM data which exhibit no peak in the entire measured q-range were plotted with $\Lambda = 0$

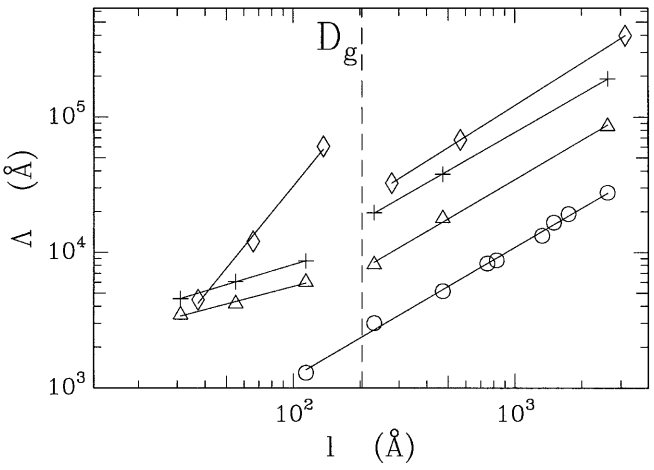

Fig. 3 Double logarithmic plot of the characteristic in-plane length Λ as a function of the prepared polymer blend film thickness *l*. The data of as prepared samples (circles), 8 h annealed samples (triangles), 62 h annealed samples (crosses) and under toluene atmosphere stored samples (rhombi) are plotted. In case of toluene vapor treatment the films are swollen, which enlarges the film thickness. The solid lines are linear fits to the data. The dashed line marks the border between 2D and 3D films D_g

dashed line now marks $D_g = 2R_g$ and thus pictures the border between 2D and 3D systems. The solid lines are fits to the data within the limited film thickness range. Within the experimental errors, the individual data sets all are describable with power laws $\Lambda(l) \sim l^{\alpha}$. Irrespective of the treatment, we obtain $\alpha = 1.0 \pm 0.07$ for the samples with $l > D_g$. As prepared samples with $l > R_g$ exhibit this exponent, too. Remarkable for $l < D_g$ the exponent is changed after a relaxation towards equilibrium. After annealing $\alpha = 0.5 \pm 0.05$ and after toluene vapor storage $\alpha = 2.0 \pm 0.08$ result. The value of $\alpha = 2.0$ is explainable within the simple spinodal dewetting model [38]. The film is destabilized by thermal fluctuations at its surface and decays into droplets. The distance d between individual droplets follows $d \sim l^2$ because the fastest growing wave vector which destroys the homogeneous film is $q_m \sim l^{-2}$. Recent investigations using grazing incidence small angle neutron scattering show that the blend film dewets the substrate. Each droplet consists of randomly arranged demixed domains [39]. In thin homopolymer films quite similar surface pattern were observed, as well [40, 41]. Thus, the distance between the droplets can be understood as the most prominent in-plane distance $\Lambda(l) = d(l)$. For morphologies created by phase separation a behavior $\Lambda \sim \chi_{eff}$ was experimentally observed [13]. Theoretically, a shift of the coexistence curve to smaller values of the inverse polymer-polymer interaction parameter χ_{eff}^{-1} with decreasing film thickness l was calculated [31]. The combination of both dependencies is in reasonable agreement with our observation. Unfortunately, no exponent α can be extracted directly due to the complication induced by the substrate (wall) interactions. Qualitatively, an increase of lateral surface structures with increasing blend film thickness was observed experimentally for different blend systems like PMMA:PS as well [9, 10]. Because in the previous literature no statistical analysis of SFM data was performed a direct comparison to our results is not possible. We interpret the observed change in the exponent α as evidence for a cross-over from a 2D to a 3D behavior of the blend film. The change resembles an enhanced domain growth in the lateral direction of the 2D films as compared to the 3D ones. Theoretically, a diverging domain size for decreasing film thickness was predicted [33]. But we do not observe the suppression of surface domains after annealing which might be due to the fact that the equilibrium structure experimentally results not from a phase separation but from a dewetting process. It should be noted that after 62 h annealing or 7 h toluene vapor treatment only a few samples with small film thickness get near their equilibrium structure. After sufficiently long annealing we always observe drop structures [8].

In summary, we have determined different film thickness dependencies of the characteristic in-plane length scale. Thus, the domain size is directly related to the film thickness. It should be noted that recently a similar power law behavior was observed in other blend systems like mixtures of brominated polystyrenes with different degrees of bromination PBr_xS:PBr_yS [42] or polystyrene blended with poly(*n*-butyl methacrylate) PS:PnBMA [43]. This suggests that the reported behavior is not limited to one special blend system only. This might have significant implication for the controlled design of surface patterns in terms of lateral size.

Acknowledgements This work was supported by the DFG Schwerpunktprogramm "Benetzung und Strukturbildung an Grenzflchen" (Sta 324/8-1).

References

1. Krausch G (1995) Mater Sci Eng R14:1
2. Krausch G (1994) Ber Bunsenges Phys Chem 98:446
3. Israelachvili JN (1991) Intermolecular and surface forces; Second edition. Academic Press, London
4. Affrossman S, O'Neill SA, Stamm M (1998) Macromolecules 31:6280
5. Dalnoki-Veress K, Forrest JA, Stevens JR, Dutcher JR (1996) J Polym Phys 34:3017
6. Emri BD, Karim A, Douglas JF (1998) J Polym Phys 36:191

7. Jandt KD, Heier J, Bates FS, Kramer EJ (1996) Langmuir 12:3716
8. Müller-Buschbaum P, O'Neill SA, Affrossman S, Stamm M (1998) Macromolecules 31:5003
9. Walheim S, Böltau M, Mlynek J, Krausch G, Steiner U (1997) Macromolecules 30:4995
10. Tanaka K, Takahara A, Kajiyama T (1996) Macromolecules 29:3232
11. Wang H, Composto RJ (2000) Europhys Lett 50:622
12. Wagner AJ, Yeomans JM (1998) Phys Rev Lett 80:1429
13. Gutmann JS, Müller-Buschbaum P, Stamm M (1999) Faraday Discuss 112:285
14. Müller-Buschbaum P, Gutmann JS, Stamm M (2000) Macromolecules 33:4886
15. Hashimoto T, Takenaka M, Jinnai H (1991) J Appl Cryst 24:457
16. Heier J, Kramer EJ, Revesz P, Battistig G, Bates FS (1999) Macromolecules 32:3758
17. Karim A, Douglas JF, Satija SK, Han CC, Goyette RJ (1999) Macromolecules 32:1119
18. Sung L, Karim A, Douglas JF, Han CC (1996) Phys Rev Lett 76:4368
19. Lawrence CJ (1988) Phys Fluids 31:2786
20. Brandrup J, Immergut EH (1989) In: Polymer Handbook, 3rd edition. John Wiley {&} Sons, New York
21. Schnell R (1997) PhD Thesis, University of Mainz
22. Müller-Buschbaum P, Gutmann JS, Stamm M (1999) J Macromol Sci B 38:577
23. Reiter G (1992) Phys Rev Lett 68:75
24. Fondecave R, Brochard-Wyart F (1998) Macromolecules 31:9305
25. Schnell R, Stamm M (1997) Physica B 234–236:247
26. Laschitsch A, Bouchard C, Habicht J, Schimmel M, Rühe J, Johannsmann D (1999) Macromolecules 32:1244
27. Visser J (1972) Adv Colloid Int Sci 3:331
28. Bornside DE, Macosko CW, Scriven LE (1991) J Electrochem Soc 138:317
29. Hall DB, Underhill P, Torkelson JM (1998) Poly Eng Sci 38:2039
30. Gu J, Bullwinkel MD, Campbell GA (1996) Poly Eng Sci 36:1019
31. Flebbe T, Dünweg B, Binder K (1996) J Phys II 6:667
32. Binder K (1999) Advances in Polymer Science 138:1
33. Fischer HP, Maass P, Dieterich W (1998) Europhys Lett 42:49
34. Bilder K (1992) Annu Rev Chem 43:33
35. Reiter G (1993) Europhys Lett 23:579
36. Keddie JL, Jones RAL, Cory RA (1994) Europhys Lett 27:59
37. Gießler KH, Rauch F, Stamm M (1994) Europhys Lett 27:605
38. Brochard-Wyart F, Redon C, Sykes C (1992) CR Acad Sci Ser 2 19:314
39. Müller-Buschbaum P, Gutmann JS, Stamm M, Cubitt R, Cunis S, von Krosigk G, Gehrke R, Petry W (2000) Physica B 283:53
40. Müller-Buschbaum P, Vanhoorne P, Scheumann V, Stamm M (1997) Europhys Lett 40:655
41. Xie R, Karim A, Douglas JF, Han CC, Weiss RA (1998) Phys Rev Lett 81:1251
42. Gutmann JS, Müller-Buschbaum P, Stamm M to be published
43. Schmitt T, Müller-Buschbaum P, Stamm M to be published